Scripta Materialia 111 (2016) 114–118

Contents lists available at ScienceDirect

Scripta Materialia

journal homepage: www.elsevier.com/locate/scriptamat

Heterogeneity in deformation of granular ceramics under dynamic loading

J.Y. Huang [a,b,c], L. Lu [a,c], D. Fan [c], T. Sun [d], K. Fezzaa [d], S.L. Xu [a,*], M.H. Zhu [b,*], S.N. Luo [c,b,*]

[a] CAS Key Laboratory of Materials Behavior and Design, Department of Modern Mechanics, University of Science and Technology of China, Hefei, Anhui 230027, PR China
[b] Key Laboratory of Advanced Technologies of Materials, Ministry of Education, Southwest Jiaotong University, Chengdu, Sichuan 610031, PR China
[c] The Peac Institute of Multiscale Sciences, Chengdu, Sichuan 610207, PR China
[d] Advanced Photon Source, Argonne National Laboratory, Argonne, IL 60439, USA

ARTICLE INFO

Article history:
Received 9 July 2015
Revised 24 August 2015
Accepted 24 August 2015
Available online 1 September 2015

Keywords:
Powder processing
Dynamic compaction
X-ray imaging
Digital image correlation
Heterogeneous deformation

ABSTRACT

Dynamic compression experiments are conducted on micron-sized SiC powders of different initial densities with a split Hopkinson pressure bar. Digital image correlation is applied to images from high-speed X-ray phase contrast imaging to map dynamic strain fields. The X-ray imaging and strain field mapping demonstrate the degree of heterogeneity in deformation depends on the initial powder density; mesoscale strain field evolution is consistent with softening or hardening manifested by bulk-scale loading curves. Statistical analysis of the strain probability distributions exhibits exponential decay tail similar to those of contact forces, which are supposed to lead to the grain-scale heterogeneity of granular materials.

Impact-induced compaction and/or sintering of powders is an important approach for synthesizing bulk ceramics, metals, alloys and composites with improved mechanical properties [1,2], and widely used in, for example, powder metallurgy [1,3,4]. The formation of a high quality compact depends on a number of factors, and identifying the important ones can help reduce undesired microstructures, including large density variations and internal cracks [5]. High strain-rate (10^2–10^3 s^{-1}) dynamic compression of granular materials, such as sand and soil, is also of interest in civil engineering [6,7]. Obtaining spatially and temporally resolved compaction dynamics in highly heterogeneous granular materials, is critical to understanding deformation mechanisms and developing constitutive models for powder compaction [5], but has been an experimental challenge.

For dynamic compression or high strain-rate loading in general, split Hopkinson pressure bar (SHPB) has been widely used for various materials including granular materials [7,8]. Strain gauges are effective for obtaining bulk, rather than meso-scale, responses. Local deformation dynamics can be characterized with two-dimensional (2D) strain field mapping, using optical digital image correlation [9] or X-ray digital image correlation (XDIC) [10,11]. XDIC is advantageous for the penetration capabilities of X-rays, and relies on images acquired with such techniques as X-ray phase contrast imaging (XPCI) [12–14]. XPCI is particularly useful to image low-*Z* powders including SiC, and the particles naturally serve as speckles. While density or particle displacement distributions under quasi-static loading have been examined to certain detail [15,16], measurements on dynamic strain distributions in ceramic powders with high-speed XDIC are extremely rare. Shock compaction experiments on powders usually yield bulk-scale stress-density relations [4,17,18] and grain-scale deformation dynamics is largely untouched [10]. Heterogeneous force distribution in granular materials (force chains) has been widely observed [19,20]. Nonetheless, heterogeneity in deformation has not been fully investigated from a quantitative point of view.

In the present study, high strain-rate compression experiments are conducted on micron-sized SiC powders of different initial densities with SHPB and high-speed XDIC. The X-ray imaging and strain field mapping demonstrate that the degree of heterogeneity in deformation depends on the initial density of a powder, and mesoscale strain field evolution is consistent with softening or hardening manifested by the bulk-scale compression curves. Statistical analysis of the strain fields reveals that the strain probability distribution follows an exponential form, similar to contact force distribution within the context of force chains [19].

SiC powder with a mean particle size of ~15 μm (Fig. 1 inset) is chosen for our dynamic compaction experiments. As shown in

* Corresponding authors at: The Peac Institute of Multiscale Sciences, Chengdu, Sichuan 610207, PR China (S.N. Luo).

E-mail addresses: slxu99@ustc.edu.cn (S.L. Xu), zhuminghao@swjtu.cn (M.H. Zhu), sluo@pims.ac.cn (S.N. Luo).

http://dx.doi.org/10.1016/j.scriptamat.2015.08.028
1359-6462/

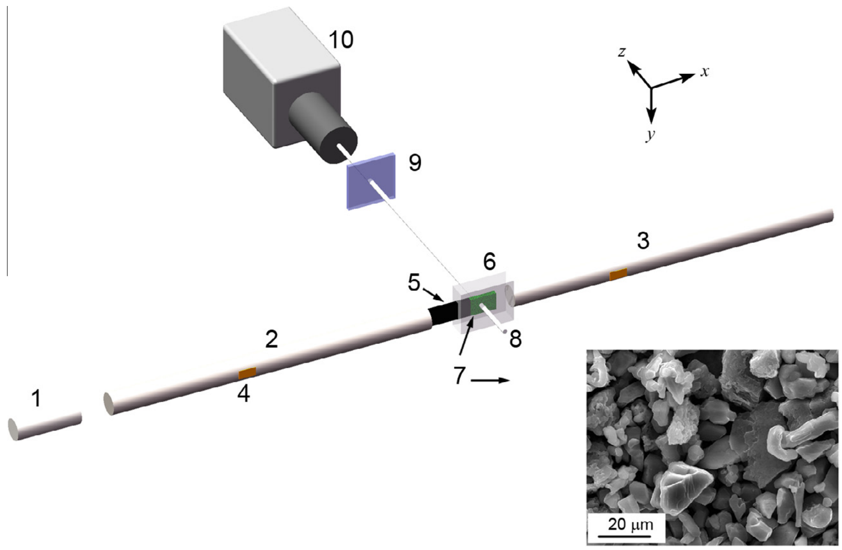

Fig. 1. Schematic diagram of the SHPB loading and high-speed X-ray imaging system. (1) Striker; (2) incident bar; (3) transmission bar; (4) strain gauges; (5) driver plate; (6) PMMA sample container; (7) powder sample; (8) X-ray beam; (9) scintillator; (10) high-speed camera. Inset: a micrograph of the SiC particles prior to impact loading.

Fig. 1, the SiC powder (7) is sandwiched between two thin polymethylmethacrylate or PMMA plates (6). The dimensions of the sample perpendicular to the X-ray (8) direction are 4 mm × 5 mm, and the thickness along the view direction is 0.5 mm. We implement a mini SHPB device along with a high-speed X-ray imaging system (8, 9, 10) at the beamline 32-ID of the Advanced Photon Source. Details of the imaging system were presented previously [13]. The striker (1), incident bar (2) and transmission bar (3) of the SHPB are all made of high-strength steel with a diameter of 4 mm. After the SHPB's gas gun is fired, impact of the striker on the incident bar generates an elastic wave propagating through the incident bar (along the x direction, Fig. 1). When the incident wave arrives at the interface between the incident bar and the steel driver plate (5), it is partially reflected owing to impedance mismatch, while the rest is transmitted into the transmission bar. The incident, reflected and transmitted waves are recorded by strain gages (4). The transmitted wave is used to calculate the stress applied to the sample (σ_s) [7], and

$$\sigma_S = E_t \varepsilon_t \frac{A_t}{A_s}, \quad (1)$$

where ε is strain, E is Young's modulus, A is cross-section area, and subscripts t and s denote the transmission bar and sample, respectively.

Since uniform deformation is usually difficult to achieve in soft/porous materials under SHPB loading, the strain calculated with incident and transmitted waves is not accurate [7]. Therefore, only stress–time curves are presented and discussed where appropriate. The incident wave signal is mainly used to trigger the high-speed camera (10). Upon loading, the X-rays transmitted through the powder sample form images on the scintillator (9) which are captured by the high-speed camera as image sequences.

Fig. 2(a) shows the stress–time curves of the two samples with different initial densities, $\rho_0 = 1.86$ g/cm^3 (densely packed, sample A) and 1.42 g/cm^3 (loosely packed, sample B). These two samples exhibit different compression responses. The axial stress in sample A increases approximately monotonically with time (t). However, the stress evolution for sample B displays three distinct stages, similar to those of aluminum foams [21]. For $t \leq 15$ μs, the curve for sample B coincides with that of sample A, showing a linear increase as expected for elastic deformation in a normal solid (stage I). The difference in wave speed due to that in the initial density is minor on the time scales of current experiments. Then the stress becomes approximately constant and even drops until a rebound at 25–30 μs (stage II), followed by a slow rise (stage III). However, the final stress level is significantly lower than that in the denser sample A.

High-speed image sequences are acquired during compression. The camera frame rate is set at 180,000 s^{-1} and the exposure time is 0.35 μs. The spatial resolution is about 2 μm. The central area (~0.5 mm × 0.5 mm) of the sample is chosen for imaging. The powder particles cannot be exactly distinguished from each other because there are about 30 layers of particles in the X-ray direction (the z-axis). The loading direction is along the x-axis. Since the X-ray intensity is not uniform across the plane of observation (the xy-plane), a flat-field correction procedure is applied to all images for better DIC analyzes [22]. The transmitted intensity field $I(x, y)$ is corrected to $I_c(x, y)$ via

$$I_c(x, y) = \frac{I(x, y)}{I_0(x, y)} I_0^*, \quad (2)$$

where $I_0(x, y)$ is the incident X-ray intensity field acquired without a sample in place, and I_0^* is the mean of the incident intensity field.

The snapshots at different instants (frames f1–f6, noted in Fig. 2(a)) after flat-field correction are shown in Fig. 2(b and c) for samples A and B, respectively. The particles in sample A are compacted uniformly across the sample. However, we observe in sample B a compaction front, propagating from the lower left to the upper right (indicated by the dashed curves in frames f3 and f4). Nonuniform compaction features appear to be more obvious in the movie (see Supplementary Materials), but are clearly identified in XDIC analyses as discussed below. The propagation velocity of the compaction front (v_{cf}) is estimated to be ~40 m/s, much higher than the impact velocity (~5 m/s). The moment when the compaction band appears in the sample actually corresponds to the inflection point of the loading curve of sample B (f3). The compaction band sweeps across the sample during the subsequent period of ~15 μs (f3–f6), corresponding to stage II on the loading curve (Fig. 2(a)). Thus, the macro stress relaxation is attributed to localized deformation in sample B. The compaction band is similar to that observed in aluminum foams [23] and porous rocks [24], which forms mainly due to inherent pore collapse. However, the intrinsic mechanism in our case is quite different, given unique microstructures of granular materials. The compaction band is not strictly parallel to the loading direction,